

Chiral four-body interactions in nuclear matter¹

N. Kaiser

Physik Department T39, Technische Universität München, D-85747 Garching, Germany

email: nkaiser@ph.tum.de

Abstract

An exploratory study of chiral four-nucleon interactions in nuclear and neutron matter is performed. The leading-order terms arising from pion-exchange in combination with the chiral 4π -vertex and the chiral $NN3\pi$ -vertex are found to be very small. Their attractive contribution to the energy per particle stays below 0.6 MeV in magnitude for densities up to $\rho = 0.4 \text{ fm}^{-3}$. We consider also the four-nucleon interaction induced by pion-exchange and twofold Δ -isobar excitation of nucleons. For most of the closed four-loop diagrams the occurring integrals over four Fermi spheres can either be solved analytically or reduced to easily manageable one- or two-parameter integrals. After summing the individually large contributions from 3-ring, 2-ring and 1-ring diagrams of alternating signs, one obtains at nuclear matter saturation density $\rho_0 = 0.16 \text{ fm}^{-3}$ a moderate contribution of 2.35 MeV to the energy per particle. The curve $\bar{E}(\rho)$ rises rapidly with density, approximately with the third power of ρ . In pure neutron matter the analogous chiral four-body interactions lead, at the same density ρ_n , to a repulsive contribution that is about half as strong. The present calculation indicates that long-range multi-nucleon forces, in particular those provided by the strongly coupled $\pi N\Delta$ -system with its small mass-gap of 293 MeV, can still play an appreciable role for the equation of state of nuclear and neutron matter.

PACS: 12.38.Bx, 21.65.+f, 24.10.Cn

1 Introduction and summary

According to their modern description and construction in chiral effective field theory, nuclear forces are organized in hierarchical way [1, 2]. For generic few-body observables the contributions arising from two-nucleon interactions are larger than those from three-nucleon forces, and the latter are again more important than possible corrections due to four-body forces. By constructing the chiral nucleon-nucleon potential up to next-to-next-to-next-leading order ($N^3\text{LO}$) one has reached in the effective field theory approach the quality of a high-precision NN-potential in reproducing empirical NN-phase shifts and deuteron properties [1, 2, 3]. By further lowering the resolution scale to $\Lambda \simeq 400 \text{ MeV}$ the chiral NN-potential can be evolved to a low-momentum NN-potential $V_{\text{low-k}}$ which becomes nearly model-independent and exhibits desirable convergence properties in perturbative calculations of many-nucleon systems and infinite nuclear matter [4, 5, 6, 7]. In chiral effective field theory the three-nucleon interaction can be constructed systematically and consistently together with the NN-potential [1, 2]. At leading order it consists of a zero-range contact-term, a mid-range 1π -exchange component and a long-range 2π -exchange component, where the parameters of the latter occur also in the subleading 2π -exchange NN-potential [5, 6]. The calculation of the subleading chiral three-nucleon force, built up by many pion-loop diagrams etc., has been completed in ref.[8]. The first calculation of the neutron matter equation of state with inclusion of these subleading chiral three-neutron interactions (at the Hartree-Fock level) has been presented recently in ref.[9].

¹Work supported in part by DFG and NSFC (CRC 110).

The leading four-nucleon interaction in chiral effective field theory has been constructed by Epelbaum in refs.[10, 11] using the method of unitary transformations. The latter method allows to project the dynamics of the interacting pion-nucleon system into the purely nucleonic subspace relevant for few-nucleon systems below the pion-production threshold. The effect of the long-range part of the chiral four-nucleon force on the ${}^4\text{He}$ nucleus has been estimated in ref.[12]. An additional binding energy of the order of a few tenth MeV has been found by computing expectations values with totally symmetric wave-functions. Phenomenological four-nucleon forces arising from pion-exchange and twofold Δ -isobar excitation of nucleons have been considered in ref.[13] for computations of four-nucleon scattering processes (n - ${}^3\text{H}$, p - ${}^3\text{He}$, n - ${}^3\text{He}$, p - ${}^3\text{H}$ and d - d). The effect of the four-nucleon force on the studied observables was found to be much smaller than that of the three-nucleon force, thus confirming the traditional belief in the hierarchical order of many-nucleon forces. However, the inclusion of the Δ -isobar was not able to resolve some longstanding discrepancies with experimental data [13].

The present paper investigates the effects of chiral four-nucleon interactions on the equation of state of homogeneous nuclear and neutron matter. The objective is to quantify those particular in-medium processes where four nucleons in the Fermi sea interact via the exchange of pions. The special case of pure neutron matter is interesting because the presence of neutral pions only leads to reduced isospin weight factors. The study of chiral four-body contributions to nuclear matter has been initiated in section 5 of ref.[14], where a particularly simple class of 2-ring Hartree diagrams (involving the chiral 4π -vertex and the chiral NN 3π -vertex) has been evaluated. With a contribution to the energy per particle of less than 0.1 MeV for densities up to twice normal nuclear matter density, $2\rho_0 = 0.32\text{ fm}^{-3}$, these long-range four-body correlations could be considered as negligibly small. In the present work we complete the leading order calculation by evaluating the corresponding Fock diagrams with one single closed nucleon ring. In addition to that we consider the four-nucleon interaction arising from pion-exchange and twofold excitation of nucleons to Δ -isobars. By introducing the direct coupling of the pion to the intermediate Δ -isobar ($\Delta\Delta\pi$ -vertex) a further type of long-range four-nucleon interaction can be generated. Although motivated more phenomenologically, these Δ -induced long-range four-nucleon interactions occur just as well in the chiral effective field theory framework. It is merely a question of how one counts the Δ -nucleon mass splitting (293 MeV), whether they are classified as leading order or as next-to-leading order terms. The calculations should be trustworthy for Fermi momenta sufficiently below the breakdown scale ~ 500 MeV of nuclear chiral effective field theory.

The present paper is organized as follows: In section 2 we evaluate the contributions to the energy per particle of isospin-symmetric nuclear matter and pure neutron matter from the leading order four-nucleon interaction (involving the chiral 4π -vertex and the chiral NN 3π -vertex). Let us note that our calculation does not follow the method of unitary transformations of ref.[11]. In this scheme iterated two-body and three-body forces give rise to induced four-body forces, whereas we restrict ourselves to four-particle irreducible diagrams related to "genuine" four-nucleon forces (called $V_{\text{class-II}}^2$ in ref.[11]). A complete study of the chiral four-body contributions to neutron matter following the method of unitary transformations has been performed recently by the Darmstadt-Ohio group [9]. Sections 3 and 4 deal with the Δ -induced four-nucleon interactions mediated by triple pion-exchange. The different orderings of the pion-couplings in the Δ -excitation-deexcitation process are combined into a symmetrized 2π or 3π contact-vertex proportional to the inverse ΔN mass-splitting or its square. Using this convenient short form we present results separately for 3-ring, 2-ring and 1-ring diagrams. In all except one case the occurring integrals over the product of four Fermi spheres can be either solved analytically or reduced to easily manageable one- or two-parameter integrals. As a major

result we find that the repulsive contribution from the dominant 3-ring diagram gets reduced to about 1/3 of its size by the (Fock-type) 2-ring and 1-ring diagrams. Altogether, there remains at saturation density $\rho_0 = 0.16 \text{ fm}^{-3}$ a contribution of $\bar{E}(\rho_0) = 2.35 \text{ MeV}$ to the energy per particle of isospin-symmetric nuclear matter. This moderate value lies on a curve for $\bar{E}(\rho)$ which however rises rapidly with density, approximately as ρ^3 . In pure neutron matter the analogous chiral four-body interactions lead, at the same density ρ_n , to a repulsive contribution that is about half as strong.

The present calculation indicates that long-range multi-nucleon forces, in particular those provided by the strongly coupled $\pi N\Delta$ -system with its small mass-gap of 293 MeV, are still of considerable size. Eventually, when combined with the relatively large attractive contributions from the subleading chiral 3N forces found in ref.[9] for pure neutron matter, one can expect cancellations to a certain degree. It remains as a future task to demonstrate these expected cancellations at a quantitative level for pure neutron matter and also for isospin-symmetric nuclear matter.

2 Leading order four-body terms related to the chiral 4π -vertex

The leading long-range four-nucleon interaction is constructed by connecting the four nucleon lines by exchanged pions which couple according to the chiral pion-pion interaction. Since the off-shell chiral 4π -vertex is involved in the process this contribution alone depends on the choice of the interpolating pion-field [11] and thus is not unique. It has to be supplemented by the four-nucleon interaction generated additionally by the chiral NN 3π -vertex, where the three pions emitted from one nucleon are absorbed on each of the other three nucleons. The sum of both pieces is actually representation-independent and thus gives rise to unique and physically meaningful results. The isovector (Weinberg-Tomozawa) NN $\pi\pi$ -vertex is proportional to the energies of the exchanged pions, which in the present application are differences of nucleon kinetic energies. According to this property the four-nucleon interaction generated by two (Weinberg-Tomozawa) NN $\pi\pi$ -vertices is a relativistic $1/M^2$ -correction. This observed suppression is equivalent to the statement $V_{\text{class-III}} = 0$ in ref.[11]. Note that we do not follow here the method of unitary transformations [11], but consider only "irreducible" diagrams, which would be commonly classified as "genuine" four-nucleon interactions. These pieces are called $V_{\text{class-II}}^2$ in ref.[11].

Fig. 1 shows the diagrams one obtains by closing the four nucleon lines to either two rings or one ring. The combinatoric factors of these diagrams are 1/8, 1/2, 1/4 and 1, respectively. Diagram with more rings are trivially zero, due to a vanishing spin-trace. For the 2-ring (Hartree) diagrams the integrals over the four Fermi spheres factorize and can be readily solved by using the master formula eq.(29) in the appendix. One finds the following contribution to the energy per particle of isospin-symmetric nuclear matter:

$$\bar{E}(\rho) = \frac{9g_A^4 m_\pi^7 u}{(4\pi f_\pi)^6} \left[u^2 - \frac{1}{2} - 2u \arctan 2u + \left(1 + \frac{1}{8u^2} \right) \ln(1 + 4u^2) \right]^2, \quad (1)$$

with the dimensionless variable $u = k_f/m_\pi$. The nucleon density ρ is related to the Fermi momentum k_f in the usual way, $\rho = 2k_f^3/3\pi^2$. The occurring parameters are: $g_A = 1.3$ (nucleon axial-vector coupling constant), $f_\pi = 92.4 \text{ MeV}$ (pion decay constant) and $m_\pi = 135 \text{ MeV}$ (neutral pion mass). Note that after adding both 2-ring diagrams in Fig. 1 the only remainder of the chiral $\pi\pi$ -interaction is a constant factor $-3m_\pi^2/f_\pi^2$. This feature has ultimately lead to

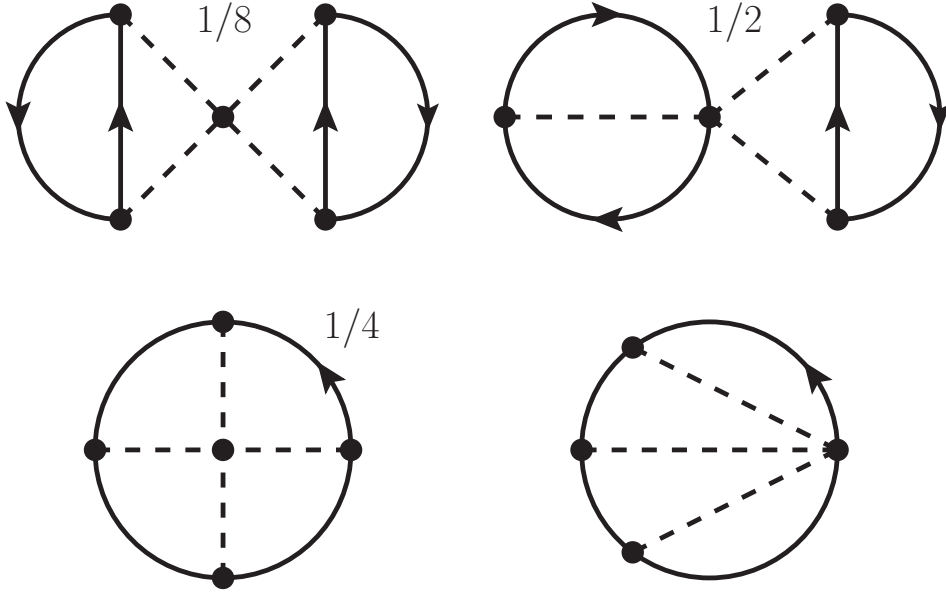


Figure 1: 2-ring and 1-ring diagrams related to the leading order (genuine) chiral four-nucleon interaction. The combinatorial factor of each diagram is specified, if it is unequal to 1.

the expression with a complete square in eq.(1). The analogous chiral four-body contribution in pure neutron matter is also of interest. In this case only neutral pions are present, which leads to a reduced isospin factor. Doing the calculation one finds from the sum of both 2-ring diagrams in Fig. 1 the following contribution to the energy per particle of pure neutron matter:

$$\bar{E}_n(\rho_n) = -\frac{3g_A^4 m_\pi^7 u}{2(4\pi f_\pi)^6} \left[u^2 - \frac{1}{2} - 2u \arctan 2u + \left(1 + \frac{1}{8u^2}\right) \ln(1 + 4u^2) \right]^2, \quad (2)$$

with $u = k_n/m_\pi$. The neutron density ρ_n is related to the neutron Fermi momentum k_n by $\rho_n = k_n^3/3\pi^2$. In order to simplify the notation, we make from here on the agreement that in all formulas for $\bar{E}_n(\rho_n)$ the dimensionless variable u has the meaning $u = k_n/m_\pi$, while in all formulas for $\bar{E}(\rho)$ it keeps its original meaning $u = k_f/m_\pi$.

The full and dashed line in Fig. 2 show these chiral four-body contributions to the equation of state of nuclear and neutron matter in the density region $0.04 \text{ fm}^{-3} < \rho, \rho_n < 0.32 \text{ fm}^{-3}$. One observes very small repulsive or attractive contributions which do not exceed 0.1 MeV in magnitude. Note that at equal densities, $\rho_n = \rho$, the isospin reduction factor $-1/6$ for pure neutron matter gets effectively compensated by the increase of the Fermi momentum k_n (by a factor $2^{1/3}$).

Next, we turn to the evaluation of the 1-ring (Fock) diagrams shown in the lower part of Fig. 1. In order to keep the symmetry of the left diagram (with a 4π -vertex), it is advantageous to add four versions of the right diagram (with a $NN3\pi$ -vertex), each then weighted by a factor $1/4$. Putting together all pieces emerging from spin- and isospin-traces, one finds the following contribution to the energy per particle of isospin-symmetric nuclear matter:

$$\begin{aligned} \bar{E}(\rho) = & \frac{3g_A^4}{16f_\pi^6 \rho} \int_{|\vec{p}_j| < k_f} \frac{d^3 p}{(2\pi)^3} \frac{1}{m_\pi^2 + \vec{q}_1^2} \frac{1}{m_\pi^2 + \vec{q}_2^2} \frac{1}{m_\pi^2 + \vec{q}_3^2} \frac{1}{m_\pi^2 + (\vec{q}_1 + \vec{q}_2 + \vec{q}_3)^2} \\ & \times \left\{ -8[\vec{q}_1 \cdot (\vec{q}_2 \times \vec{q}_3)]^2 + m_\pi^2 \left[-4\vec{q}_1^2 \vec{q}_3^2 - 4\vec{q}_1^2 (\vec{q}_2^2 + \vec{q}_1 \cdot \vec{q}_3) \right. \right. \\ & \left. \left. + 2\vec{q}_1^2 \vec{q}_2 \cdot (2\vec{q}_1 - 5\vec{q}_3) + 8(\vec{q}_1 \cdot \vec{q}_2)^2 + \vec{q}_1 \cdot \vec{q}_3 \vec{q}_2 \cdot (8\vec{q}_1 + 3\vec{q}_2) - 6\vec{q}_1 \cdot \vec{q}_2 \vec{q}_2 \cdot \vec{q}_3 \right] \right\}, \quad (3) \end{aligned}$$

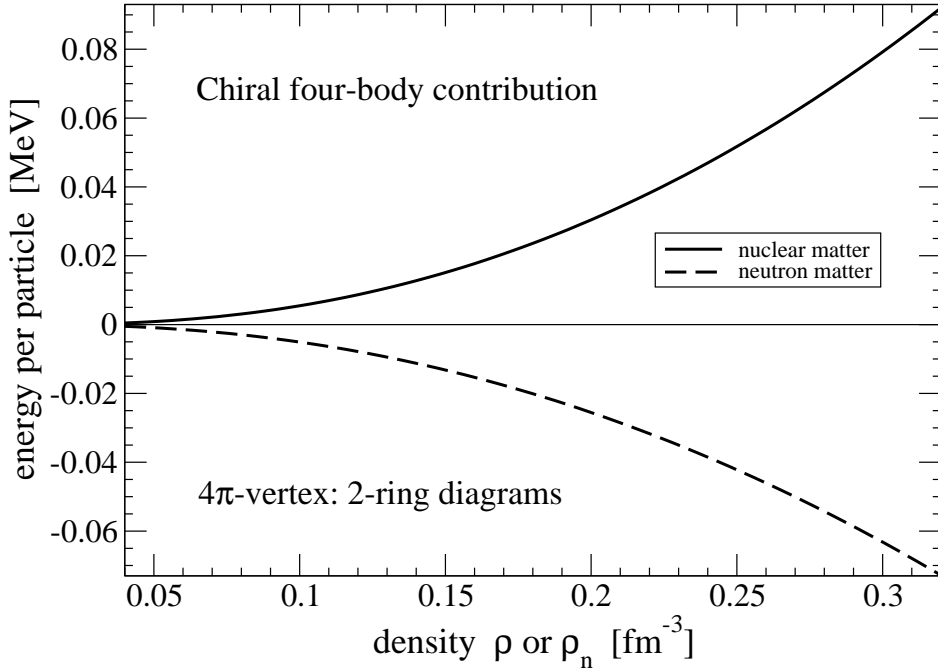


Figure 2: Chiral four-body contributions to the energy per particle of nuclear and neutron matter arising from leading order 2-ring diagrams.

with momentum transfers $\vec{q}_1 = \vec{p}_1 - \vec{p}_4$, $\vec{q}_2 = \vec{p}_2 - \vec{p}_1$ and $\vec{q}_3 = \vec{p}_3 - \vec{p}_2$. In the case of pure neutron matter, where the chiral four-body interaction is mediated by neutral pions only, one gets from the sum of the 1-ring diagrams:

$$\begin{aligned} \bar{E}_n(\rho_n) = & \frac{g_A^4 m_\pi^2}{32 f_\pi^6 \rho_n} \int_{|\vec{p}_j| < k_n} \frac{d^{12}p}{(2\pi)^{12}} \frac{1}{m_\pi^2 + \vec{q}_1^2} \frac{1}{m_\pi^2 + \vec{q}_2^2} \frac{1}{m_\pi^2 + \vec{q}_3^2} \\ & \times \frac{1}{m_\pi^2 + (\vec{q}_1 + \vec{q}_2 + \vec{q}_3)^2} \left\{ \vec{q}_2^2 \vec{q}_1 \cdot \vec{q}_3 - 2\vec{q}_2 \cdot \vec{q}_3 (\vec{q}_1 + \vec{q}_2) \cdot \vec{q}_1 \right\}. \end{aligned} \quad (4)$$

Note that we have exploited the symmetry under the interchange $\vec{q}_1 \leftrightarrow \vec{q}_3$ in order to simplify the expressions in the curly brackets of eqs.(3,4). The occurrence of a product of four different pion-propagators prohibits any substantial analytical reduction of these 12-dimensional integrals over the product of four Fermi spheres. Note also that there is a marked difference between $\bar{E}(\rho)$ in eq.(3) and $\bar{E}_n(\rho_n)$ in eq.(4). After adding both 1-ring diagrams the result for pure neutron matter becomes proportional to m_π^2 , while there remains a finite term $-8[\vec{q}_1 \cdot (\vec{q}_2 \times \vec{q}_3)]^2$ for isospin-symmetric nuclear matter even in the chiral limit $m_\pi = 0$. For comparison, the sum of the 2-ring (Hartree) diagrams has generated the m_π^2 factor in both cases. We note as an aside that in the chiral limit, $m_\pi = 0$, eq.(3) leads to the result $\bar{E}(\rho) \simeq -1.13 g_A^4 k_f^7 / (4\pi f_\pi)^6$ with a simple seventh power dependence on the Fermi momentum k_f .

The full and dashed line in Fig. 3 show the numerical results for the 1-ring (Fock) contributions as a function of the density, ρ or ρ_n . In the case of pure neutron matter one finds the usual pattern with the Fock contribution having opposite sign and reduced spin-weight in comparison to the Hartree contribution (shown in Fig. 2). In contrast to this the Fock contribution for isospin-symmetric nuclear matter is about a factor of five larger (and of opposite sign) than the Hartree contribution. This reversed ordering comes from the fact that the Hartree contribution eq.(1) is “accidentally” suppressed by a factor $(m_\pi/k_f)^2$, while the Fock contribution remains finite in the chiral limit $m_\pi = 0$. The Hartree terms shown in Fig. 2 are therefore not representative for the size of chiral four-body contributions. Irrespective of that exceptional behavior,

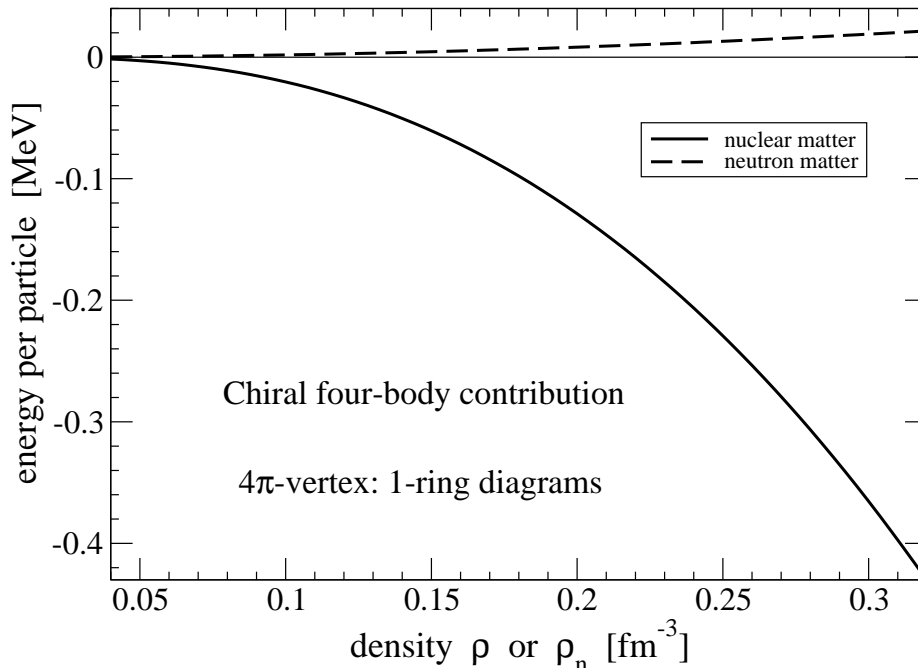


Figure 3: Chiral four-body contributions to the energy per particle of nuclear and neutron matter arising from leading order 1-ring diagrams.

the attractive chiral four-body contributions represented by the diagrams in Fig. 1 stay in total below 0.6 MeV for densities up to $\rho = 0.4 \text{ fm}^{-3}$. For this reason they can be considered as negligibly small.

Let us remark that in the case of pure neutron matter the method of unitary transformations [11] provides just one additional leading order chiral four-body interaction (called V^a in ref.[9]). It has been computed in ref.[9] with the result that its contribution to the energy per particle $\bar{E}_n(\rho_n)$ reaches about -0.25 MeV at a density of $\rho_n = 0.2 \text{ fm}^{-3}$.

3 Single delta-isobar excitation on two nucleons

In this section we consider a more relevant type of long-range four-nucleon interaction [13]. It arises from triple pion-exchange and the excitation of two nucleons into virtual Δ -isobars. The corresponding four-nucleon interaction is depicted by the left diagram in Fig. 4. For an efficient treatment it is advantageous to combine the direct and crossed $\pi N \rightarrow \Delta \rightarrow \pi N$ transition into a contact-vertex for the absorbed and emitted pion. In the present application the energy dependence of the Δ -propagator $i(\omega - \Delta)^{-1}$ can be neglected since the energies ω carried by the virtual pions are differences of small nucleon kinetic energies. With this valid approximation the pertinent contact-vertex reads:

$$\frac{ig_A^2}{f_\pi^2 \Delta} \left[\delta_{ab} \vec{q}_a \cdot \vec{q}_b - \frac{1}{4} \epsilon_{abc} \tau_c \vec{\sigma} \cdot (\vec{q}_a \times \vec{q}_b) \right], \quad (5)$$

where \vec{q}_a is an ingoing and \vec{q}_b is an outgoing pion-momentum. We have inserted in eq.(5) already the empirically well-satisfied coupling constant ratio $g_{\pi N \Delta} / g_{\pi NN} = 3/\sqrt{2}$, and $\Delta = 293 \text{ MeV}$ denotes the mass-splitting between the Δ -isobar and the nucleon. Note that the scale $\Delta = 293 \text{ MeV}$ is comparable to the Fermi momentum $k_{f0} = 263 \text{ MeV}$ at nuclear matter saturation density $\rho_0 = 0.16 \text{ fm}^{-3}$. At $\rho_n = 2\rho_0$ the neutron Fermi momentum $k_n = 418 \text{ MeV}$ exceeds the scale $\Delta = 293 \text{ MeV}$ already considerably. For the in-medium interaction the momenta of

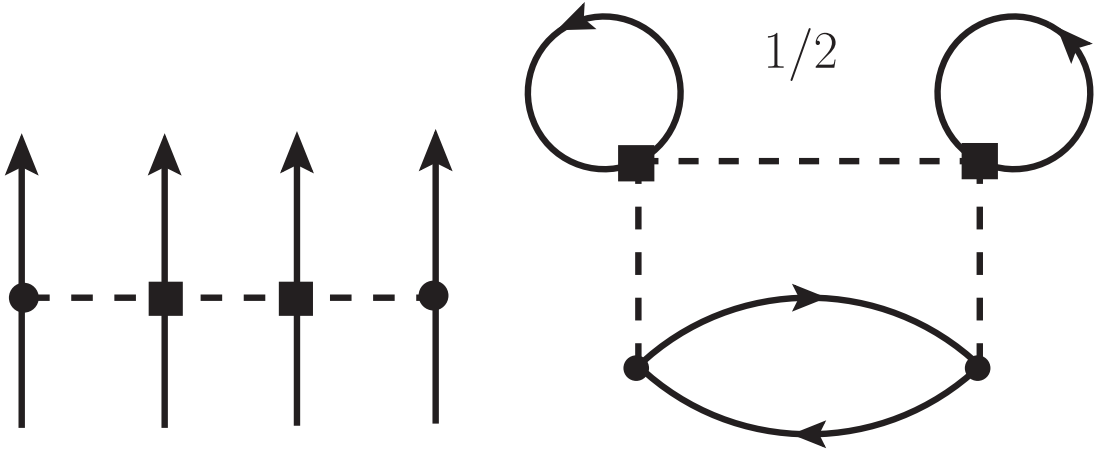


Figure 4: Left: Long-range four-nucleon interaction with twofold Δ -isobar excitation. Right: Corresponding 3-ring Hartree diagram with combinatorial factor $1/2$.

the exchanged pions vary over the range $0 < |\vec{q}_{a,b}| < 2k_{f,n}$, but the included high-momentum part receives very little weight in the Fermi sphere integrals (as demonstrated in the appendix). When working with a $NN\pi\pi$ contact-vertex the task of enumerating all topologically distinct in-medium diagrams gets simplified a lot. We turn now to the analytical evaluation of the pertinent four-loop in-medium diagrams representing the energy density, $\rho\bar{E}(\rho)$ or $\rho_n\bar{E}_n(\rho_n)$.

3.1 Three-ring diagram

This simplest closed in-medium diagram resulting from the Δ -induced four-nucleon interaction is the 3-ring diagram shown in the right part of Fig. 4. The upper two loops produce each a factor of density, ρ or ρ_n , and the remaining integral over two Fermi spheres is readily solved by using eq.(29). One finds the following contributions to the energy per particle of isospin-symmetric nuclear matter:

$$\bar{E}(\rho) = \frac{g_A^6 m_\pi^9 u^3}{(2\pi f_\pi)^6 \Delta^2} \left\{ \frac{16u^6}{9} - 12u^4 + \frac{20u^2}{3} + \frac{70u^3}{3} \arctan 2u - \left(12u^2 + \frac{5}{3} \right) \ln(1 + 4u^2) \right\}, \quad (6)$$

and pure neutron matter:

$$\bar{E}_n(\rho_n) = \frac{g_A^6 m_\pi^9 u^3}{(2\pi f_\pi)^6 \Delta^2} \left\{ \frac{4u^6}{27} - u^4 + \frac{5u^2}{9} + \frac{35u^3}{18} \arctan 2u - \left(u^2 + \frac{5}{36} \right) \ln(1 + 4u^2) \right\}, \quad (7)$$

where the latter differs from the former only by an isospin reduction factor $1/12$ (at equal Fermi momenta, $k_n = k_f$).

Fig. 5 shows the four-body contributions to the energy per particle of nuclear and neutron matter as they arise from the 3-ring diagram with twofold Δ -excitation. For isospin-symmetric nuclear matter (see full line) one obtains a sizeable repulsion which reaches a value of 74 MeV at twice normal nuclear matter density $2\rho_0 = 0.32 \text{ fm}^{-3}$. At saturation density $\rho_0 = 0.16 \text{ fm}^{-3}$ the corresponding value $\bar{E}(\rho_0) = 7.42 \text{ MeV}$ is ten times smaller, but this amounts still to almost half of the empirical nuclear matter binding energy $\bar{E}_0 \simeq -16 \text{ MeV}$. The dashed curve in Fig. 5 for pure neutron matter lies about 20% below the full curve for isospin-symmetric nuclear matter. This feature demonstrates that the isospin reduction factor $1/12$ in eq.(7) gets to a large extent compensated by the increase of the neutron Fermi momentum k_n .

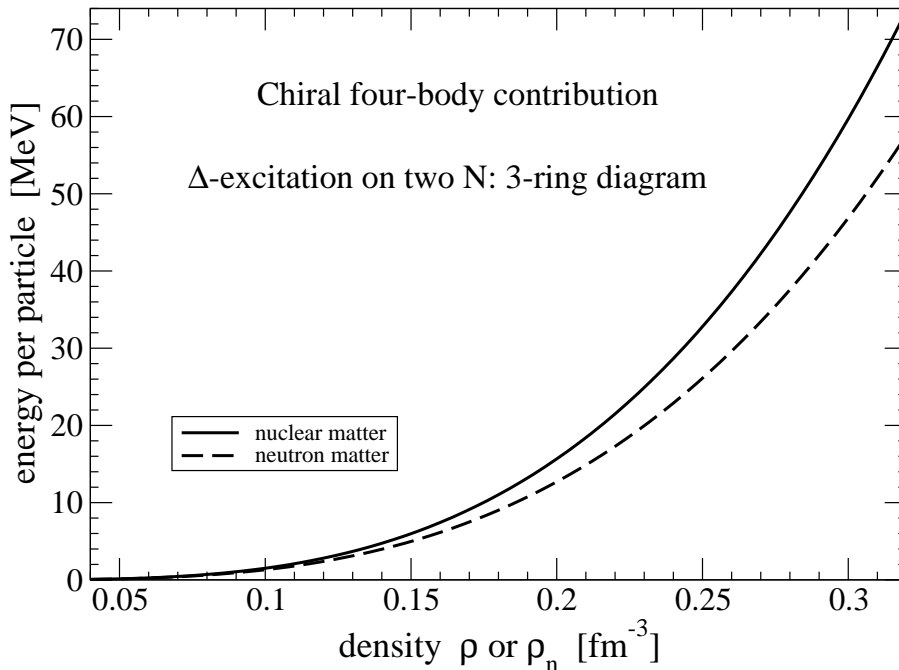


Figure 5: Δ -induced chiral four-body contributions to the energy per particle of nuclear and neutron matter: 3-ring diagram.

With the analytical formulas eqs.(6,7) and the corresponding numerical results displayed in Fig. 5 the size of long-range Δ -induced four-nucleon contributions in nuclear and neutron matter is set. From here on the interesting question is, how much of a reduction will be provided by the Fock-type diagrams with fewer rings.

3.2 Two-ring diagrams

The 2-ring diagrams resulting from the chiral four-nucleon interaction with twofold Δ -isobar excitation are shown in Fig. 6. The last two diagrams (marked by 0) vanish identically. The upper diagram of this subset involves a central pion which carries zero-momentum and therefore does not couple according to the contact-vertex eq.(5). In order not to vanish in the first step, the spin-traces in the lower diagram select from the contact-vertex eq.(5) the spin-dependent part. Furthermore, by taking into account momentum conservation at each vertex one obtains a scalar triple product of three linearly dependent vectors ($\vec{q}_1 + \vec{q}_2 + \vec{q}_3 = \vec{0}$), which vanishes identically.

Obviously, the upper two (topologically distinct) diagrams in Fig. 6 give rise to equal contributions. The left loop produces just a factor of density and the Fermi sphere integrals over the pion-propagators and momentum-dependent interactions on the right can be factorized with the help of tensors. Performing this strategy, as outlined in eq.(30) of the appendix, one ends up with the following expressions for the contributions to the energy particle of nuclear and neutron matter:

$$\bar{E}(\rho) = -\frac{g_A^6 m_\pi^9}{4(2\pi f_\pi)^6 \Delta^2} \int_0^u dx \left[2G_S(x)H_S(x) + G_T(x)H_T(x) \right], \quad (8)$$

$$\bar{E}_n(\rho_n) = -\frac{g_A^6 m_\pi^9}{24(2\pi f_\pi)^6 \Delta^2} \int_0^u dx \left[G_S(x)H_S(x) + 2G_T(x)H_T(x) \right]. \quad (9)$$

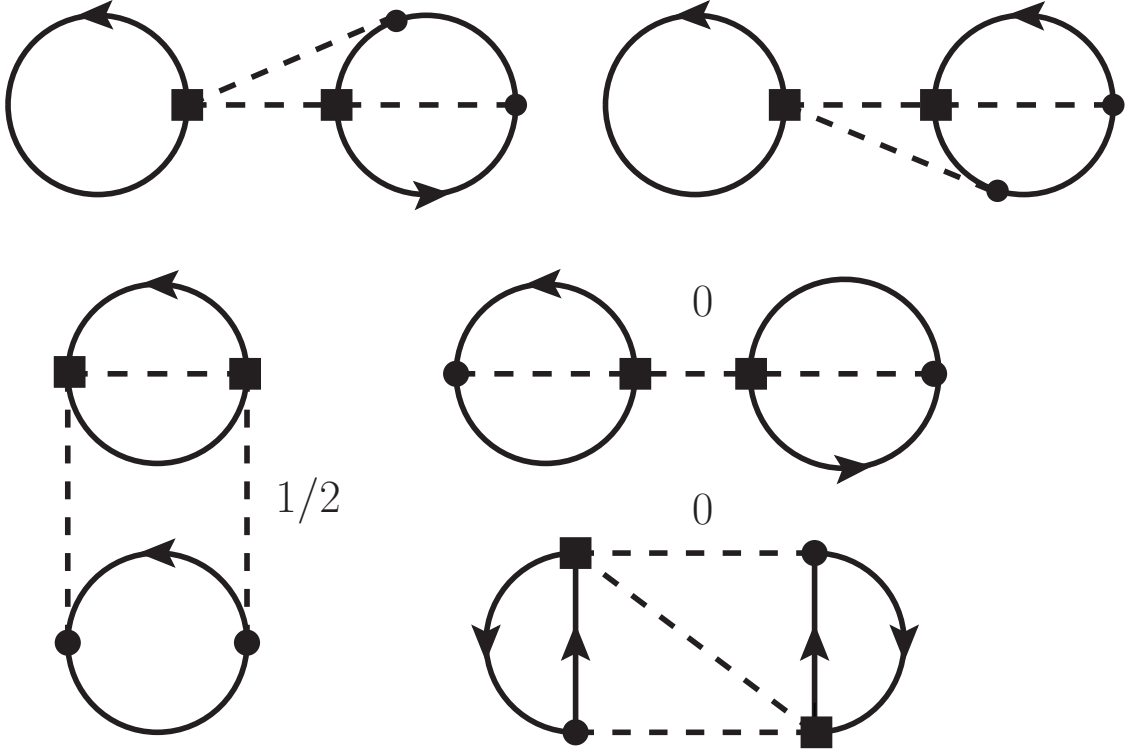


Figure 6: 2-ring diagrams resulting from the chiral four-nucleon interaction with twofold Δ -isobar excitation.

Here, we have introduced the auxiliary functions:

$$\begin{aligned}
G_S(x) &= \frac{4ux}{3}(2u^2 - 3) + 4x \left[\arctan(u+x) + \arctan(u-x) \right] \\
&\quad + (x^2 - u^2 - 1) \ln \frac{1 + (u+x)^2}{1 + (u-x)^2},
\end{aligned} \tag{10}$$

$$\begin{aligned}
G_T(x) &= \frac{ux}{6}(8u^2 + 3x^2) - \frac{u}{2x}(1 + u^2)^2 + \frac{1}{8} \left[\frac{(1 + u^2)^3}{x^2} \right. \\
&\quad \left. - x^4 + (1 - 3u^2)(1 + u^2 - x^2) \right] \ln \frac{1 + (u+x)^2}{1 + (u-x)^2},
\end{aligned} \tag{11}$$

defined by the tensorial Fermi sphere integral in eq.(30) of the appendix. The other auxiliary functions $H_{S,T}(x)$ occurring in eqs.(8,9) are closely related to $G_{S,T}(x)$:

$$H_S(x) = \frac{5}{2}G_S(x) + 2ux(1 - 2u^2) + \frac{1}{2}(u^2 - x^2 - 1) \ln \frac{1 + (u+x)^2}{1 + (u-x)^2}, \tag{12}$$

$$H_T(x) = G_T(x) + \frac{ux}{2} - \frac{3u}{2x}(1 + u^2) + \frac{1}{8} \left[\frac{3}{x^2}(1 + u^2)^2 + 2 - 2u^2 - x^2 \right] \ln \frac{1 + (u+x)^2}{1 + (u-x)^2}. \tag{13}$$

The lower left 2-ring diagram in Fig.6 (with a combinatorial factor 1/2) is more difficult to evaluate. In order to facilitate an analytical treatment one chooses the momentum transfers carried by the exchanged pions as the basic variables and works with integrals over shifted Fermi spheres. In the end one arrives at a double-integral representation for the contributions

to the energy particle of nuclear and neutron matter:

$$\begin{aligned} \bar{E}(\rho) = & \frac{g_A^6 m_\pi^9}{(2\pi f_\pi)^6 \Delta^2 u^3} \int_0^u dx \int_0^u dy \frac{x^3(u^2 - y^2)}{(1 + 4x^2)^2} (u - x)^2 (2u + x) \left\{ 7xy(1 + 4y^2)^2 \right. \\ & + 16x^3 \left[10y - \frac{136y^3}{3} - 7x^2y - 5 \arctan(2x + 2y) + 5 \arctan(2x - 2y) \right] \\ & \left. + \frac{1}{16}(4x^2 - 4y^2 - 1) [7(1 + 4y^2)^2 + 8x^2(14x^2 - 28y^2 - 13)] \ln \frac{1 + 4(x + y)^2}{1 + 4(x - y)^2} \right\}, \quad (14) \end{aligned}$$

$$\begin{aligned} \bar{E}_n(\rho_n) = & \frac{g_A^6 m_\pi^9}{3(2\pi f_\pi)^6 \Delta^2 u^3} \int_0^u dx \int_0^u dy \frac{x^3(u^2 - y^2)}{(1 + 4x^2)^2} (u - x)^2 (2u + x) \\ & \times \left\{ 4xy(1 + 4y^2)^2 + 32x^3 \left[2y - \frac{32y^3}{3} - 2x^2y - \arctan(2x + 2y) \right. \right. \\ & \left. \left. + \arctan(2x - 2y) \right] + \frac{1}{4}(4x^2 - 4y^2 - 1)^3 \ln \frac{1 + 4(x + y)^2}{1 + 4(x - y)^2} \right\}. \quad (15) \end{aligned}$$

By inspecting the first lines in eqs.(14,15) one realizes that the master integral eq.(29) has been employed. In addition to that, the following reduction formula has helped to eliminate a complicated angular integral:

$$\int_0^u dp \int_{-1}^1 dz p^2 F(pz + \sqrt{u^2 - p^2(1 - z^2)}) = \int_0^u dy (u^2 - y^2) F(2y), \quad (16)$$

where the argument of $F(\dots)$ on the left hand side gives the distance to the boundary of a shifted Fermi sphere, with p being the displacement of the center. We have checked numerically the analytical expressions in eqs.(14,15) against the original (untreated) four Fermi sphere integrals and found good agreement. The advantage of the double-integral representations for $\bar{E}(\rho)$ and $\bar{E}_n(\rho_n)$ in eqs.(14,15) is that these can be evaluated with much higher numerical precision.

The full and dashed line in Fig. 7 show the Δ -induced chiral four-body contributions to the energy per particle of nuclear and neutron matter as they arise from the 2-ring diagrams. The first part given by eqs.(8,9) is typically a factor 3 to 4 larger than the second part given by eqs.(14,15) and both pieces come with the same sign. By comparison with Fig. 5 one observes that the individually large contributions from the 3-ring and 2-ring diagrams nearly cancel each other, leaving a small repulsive (attractive) remainder for nuclear (neutron) matter. In magnitude this remainder is only about 1/7 of the starting values. As a consequence of this feature the final result for the Δ -induced chiral four-body contributions will be determined in a crucial way by the 1-ring diagrams.

3.3 One-ring diagrams

The 1-ring diagrams resulting from the chiral four-nucleon interaction with twofold Δ -isobar excitation are shown in Fig. 8. For the first diagram with a U-shaped pion-line three of the four occurring Fermi sphere integrals over the pion-propagators are structurally equivalent and with inclusion of the momentum-dependent interactions they factorize with the help of tensors. In the end only one single radial integral remains and the corresponding contributions to the energy per particle of nuclear and neutron matter read:

$$\bar{E}(\rho) = \frac{g_A^6 m_\pi^9}{8(4\pi f_\pi)^6 \Delta^2 u^3} \int_0^u dx \frac{1}{x} \left[8G_S^3(x) + 9G_S(x)G_T^2(x) + G_T^3(x) \right], \quad (17)$$

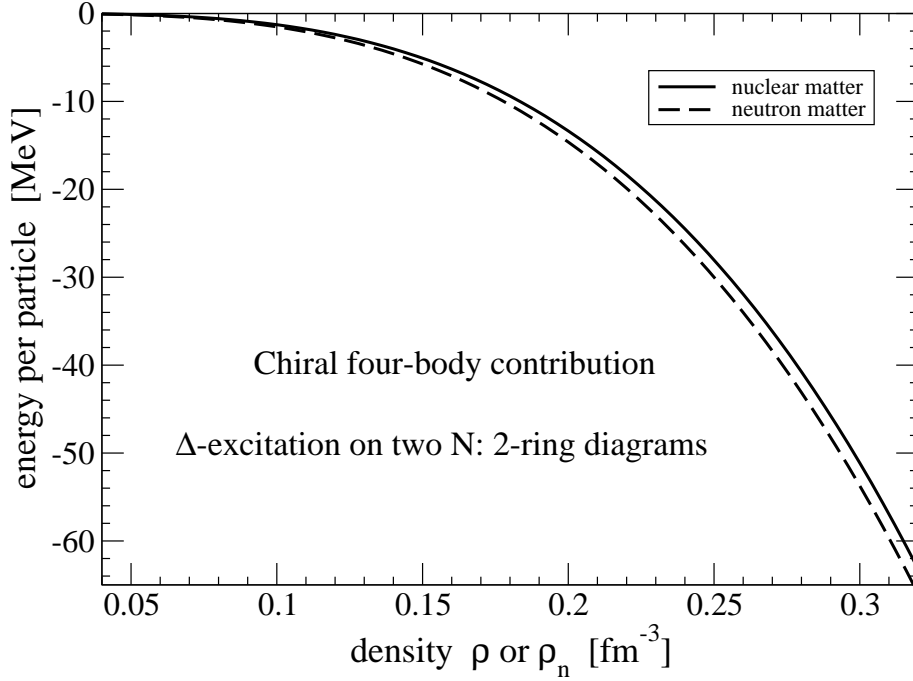


Figure 7: Δ -induced chiral four-body contributions to the energy per particle of nuclear and neutron matter: 2-ring diagrams.

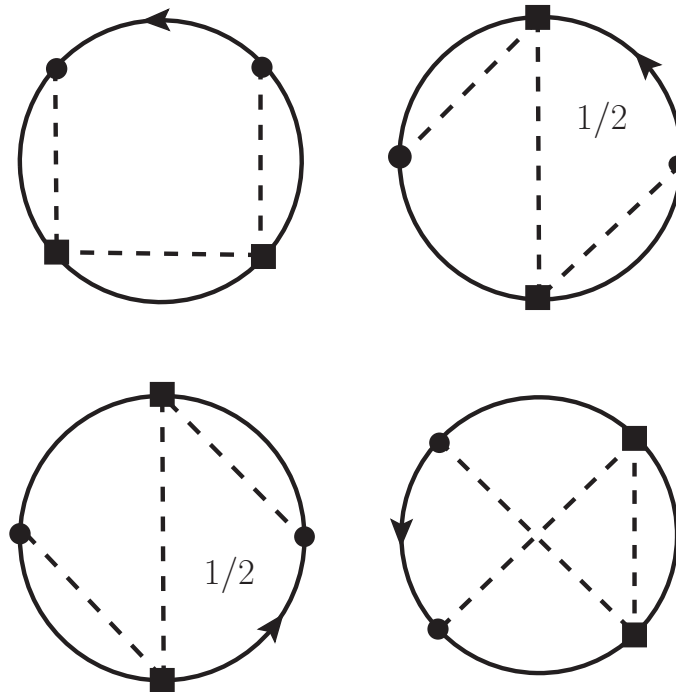


Figure 8: 1-ring diagrams resulting from the chiral four-nucleon interaction with twofold Δ -isobar excitation.

$$\bar{E}_n(\rho_n) = \frac{g_A^6 m_\pi^9}{12(4\pi f_\pi)^6 \Delta^2 u^3} \int_0^u dx \frac{1}{x} \left[G_S^3(x) + 6G_S(x)G_T^2(x) + 2G_T^3(x) \right], \quad (18)$$

with the auxiliary functions $G_{S,T}(x)$ given in eqs.(10,11). The next two (topologically distinct) 1-ring diagrams in Fig. 8 have a pion-line running zig-zag. Since both give equal contributions their combinatorial factor 1/2 gets effectively compensated. Again, the Fermi sphere integrals over the pion-propagators associated to the short pion-lines factorize via tensors. For the remaining integral over two Fermi spheres $|\vec{p}_{1,2}| < k_f$ the angular integrations can be carried out and in this procedure the third pion-propagator introduces the logarithmic function:

$$L = \ln \frac{1 + (x + y)^2}{1 + (x - y)^2}. \quad (19)$$

Putting all pieces together and exploiting the symmetry under the interchange $x \leftrightarrow y$, one finds the following double-integral representations for the contributions of the zig-zag 1-ring diagrams to the energy per particle of nuclear and neutron matter:

$$\begin{aligned} \bar{E}(\rho) &= \frac{g_A^6 m_\pi^9}{(4\pi f_\pi)^6 \Delta^2 u^3} \int_0^u dx \int_0^u dy \left\{ 2G_S(x)G_S(y) [4xy - L] + G_S(x)G_T(y) \right. \\ &\quad \times \left[5xy - \frac{3x}{y}(1+x^2) + \frac{L}{4} \left(\frac{3}{y^2}(1+x^2)^2 - 2 - 6x^2 + 3y^2 \right) \right] + G_T(x)G_T(y) \\ &\quad \left. \times \left[\frac{xy}{8} + \frac{3}{8y} \left(\frac{3}{2x} + 2x - x^3 \right) + \frac{L}{32} \left(\frac{3}{y^2}(x^4 - x^2 - 5 - \frac{3}{2x^2}) - 1 - 3x^2 \right) \right] \right\}, \quad (20) \end{aligned}$$

$$\begin{aligned} \bar{E}_n(\rho_n) &= \frac{g_A^6 m_\pi^9}{6(4\pi f_\pi)^6 \Delta^2 u^3} \int_0^u dx \int_0^u dy \left\{ G_S(x)G_S(y) [4xy - L] + G_S(x)G_T(y) \right. \\ &\quad \times \left[10xy - \frac{6x}{y}(1+x^2) + \frac{L}{2} \left(\frac{3}{y^2}(1+x^2)^2 - 2 - 6x^2 + 3y^2 \right) \right] + G_T(x)G_T(y) \\ &\quad \left. \times \left[xy + \frac{3}{y} \left(\frac{3}{2x} + 2x - x^3 \right) + \frac{L}{4} \left(\frac{3}{y^2}(x^4 - x^2 - 5 - \frac{3}{2x^2}) - 1 - 3x^2 \right) \right] \right\}. \quad (21) \end{aligned}$$

The last 1-ring diagram in Fig. 8 involves crossed pion lines. The assignment of momenta to the virtual pions is now such that the previous factorization procedure does not work anymore. From the four Fermi sphere integrals only the one associated to the nucleon line between the contact-vertices can be performed analytically and the contributions to the energy per particle of nuclear and neutron matter read:

$$\begin{aligned} \bar{E}(\rho) &= \frac{3g_A^6}{32f_\pi^6 \Delta^2 u^3} \int_{|\vec{p}_j| < k_f} \frac{d^9 p}{(2\pi)^9} \frac{\vec{q}_1^2}{(m_\pi^2 + \vec{q}_1^2)(m_\pi^2 + \vec{q}_2^2)|\vec{\eta}|} \\ &\quad \times \left\{ \vec{q}_2^2 [G_S(|\vec{\eta}|) - G_T(|\vec{\eta}|)] + \frac{3}{\vec{\eta}^2} (\vec{\eta} \cdot \vec{q}_2)^2 G_T(|\vec{\eta}|) \right\}, \quad (22) \end{aligned}$$

$$\begin{aligned} \bar{E}_n(\rho_n) &= \frac{g_A^6}{32f_\pi^6 \Delta^2 u^3} \int_{|\vec{p}_j| < k_n} \frac{d^9 p}{(2\pi)^9} \frac{\vec{q}_1 \cdot \vec{q}_2}{(m_\pi^2 + \vec{q}_1^2)(m_\pi^2 + \vec{q}_2^2)|\vec{\eta}|} \\ &\quad \times \left\{ \vec{q}_1 \cdot \vec{q}_2 [G_S(|\vec{\eta}|) - G_T(|\vec{\eta}|)] + \frac{3}{\vec{\eta}^2} \vec{\eta} \cdot \vec{q}_1 \vec{\eta} \cdot \vec{q}_2 G_T(|\vec{\eta}|) \right\}, \quad (23) \end{aligned}$$

with momentum transfers $\vec{q}_1 = \vec{p}_1 - \vec{p}_3$, $\vec{q}_2 = \vec{p}_2 - \vec{p}_3$ and the vector $\vec{\eta} = (\vec{p}_1 + \vec{p}_2 - \vec{p}_3)/m_\pi$.

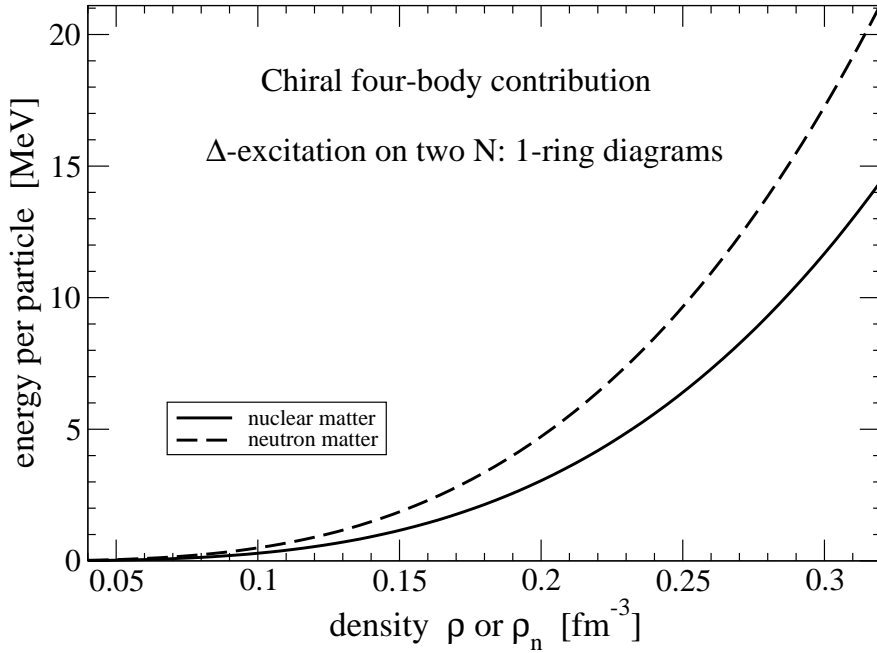


Figure 9: Δ -induced chiral four-body contributions to the energy per particle of nuclear and neutron matter: 1-ring diagrams.

The full and dashed line in Fig. 9 show the Δ -induced chiral four-body contributions to the energy per particle of nuclear and neutron matter as they arise from the 1-ring diagrams. The three pieces (with U-shaped, zig-zag and crossed pion-lines) provide approximately equal amounts. As expected the sign of $\bar{E}(\rho)$ and $\bar{E}_n(\rho_n)$ is opposite to the contributions from the 2-ring diagrams shown in Fig. 7. Although the magnitude of the repulsive 1-ring contributions is substantially reduced (by a factor 3 to 4) in comparison to the previous terms, these are by no means small. Such strongly with density rising four-body correlations, which reach values of 14.4 MeV or 21.2 MeV at $2\rho_0 = 0.32 \text{ fm}^{-3}$, affect the equation of state of nuclear or neutron matter appreciably.

4 Double delta-isobar excitation on one nucleons

In this section we consider a further type of Δ -induced long-range four-nucleon interaction [13]. Once the Δ -isobar is excited, it can also couple directly to the pion (through the $\Delta\Delta\pi$ -vertex). Each of the three pions emitted from the central nucleon gets absorbed on a spectator nucleon. For an efficient treatment of this chiral four-nucleon interaction it is advantageous to condense the three-pion dynamics at the central nucleon into a symmetrized three-pion contact-vertex as symbolized in Fig. 10. Approximating the Δ -propagator by the inverse mass-splitting $-i/\Delta$ and summing over all six permutations of (a, b, c) the pertinent NN3 π contact-vertex reads:

$$\frac{g_A^3}{40f_\pi^3\Delta^2} \left\{ -75\epsilon_{abc} \vec{q}_a \cdot (\vec{q}_b \times \vec{q}_c) + \vec{q}_a \cdot \vec{q}_b \vec{\sigma} \cdot \vec{q}_c (18\delta_{ab}\tau_c - 7\delta_{ac}\tau_b - 7\delta_{bc}\tau_a) \right. \\ \left. + \vec{q}_a \cdot \vec{q}_c \vec{\sigma} \cdot \vec{q}_b (18\delta_{ac}\tau_b - 7\delta_{ab}\tau_c - 7\delta_{bc}\tau_a) + \vec{q}_b \cdot \vec{q}_c \vec{\sigma} \cdot \vec{q}_a (18\delta_{bc}\tau_a - 7\delta_{ac}\tau_b - 7\delta_{ab}\tau_c) \right\}, \quad (24)$$

where \vec{q}_a, \vec{q}_b and \vec{q}_c denote outgoing pion-momenta. In order to fix the $\Delta\Delta\pi$ -vertex we use the coupling constant ratio $g_{\pi\Delta\Delta}/g_{\pi NN} = 1/5$ of the quark-model. The relation for isospin (transition) operators, $T_a\Theta_bT_c^\dagger = (5i\epsilon_{abc} - \delta_{ab}\tau_c + 4\delta_{ac}\tau_b - \delta_{bc}\tau_a)/3$, with Θ_b the 4×4 Δ -isospin matrices has been employed together with an analogous relation for spin (transition) operators.

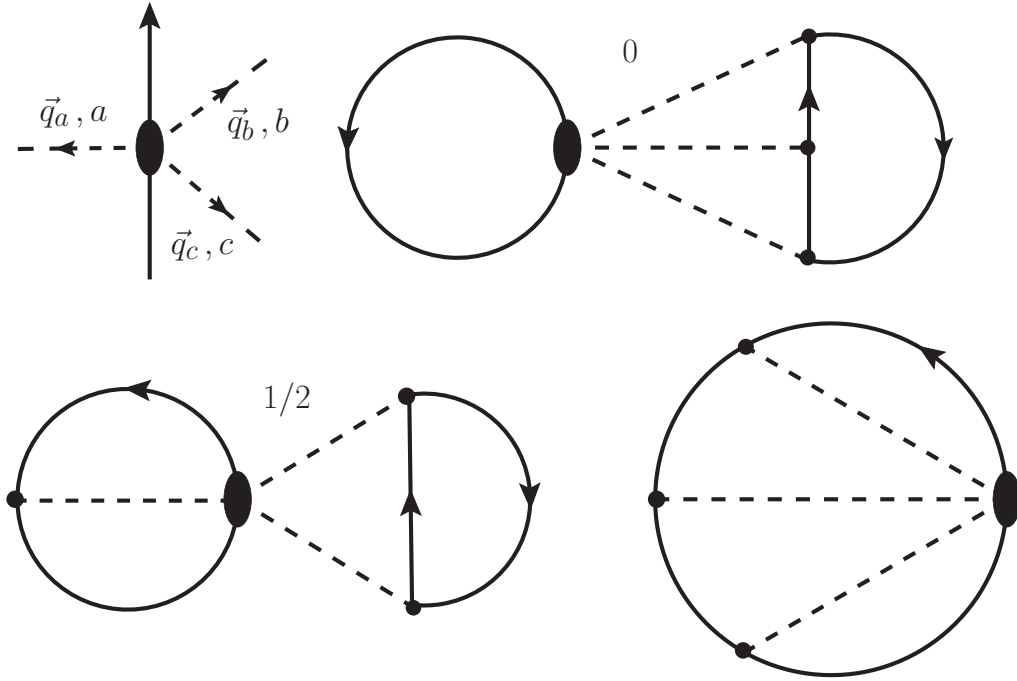


Figure 10: The filled ellipse symbolizes the symmetrized three-pion contact-vertex involving double Δ -excitation. The associated chiral four-nucleon interaction gives rise to one non-vanishing 2-ring diagram and one non-vanishing 1-ring diagram.

The 2-ring and 1-ring diagrams resulting from the three-pion contact-vertex are shown in Fig. 10. The upper 2-ring diagram vanishes because the spin-trace (on the left) selects the term proportional to the scalar triple product from eq.(24) with linearly dependent vectors ($\vec{q}_a + \vec{q}_b + \vec{q}_c = \vec{0}$). For the lower 2-ring diagram (with combinatoric factor 1/2) the integrals over the Fermi sphere factorize and can be solved by using the master formula eq.(29). The corresponding contributions to the energy per particle of nuclear and neutron matter read:

$$\begin{aligned} \bar{E}(\rho) &= \frac{5g_A^6 m_\pi^9 u}{3(4\pi f_\pi)^6 \Delta^2} \left[\frac{4u^4}{3} - 6u^2 + 2 + 10u \arctan 2u - \left(\frac{9}{2} + \frac{1}{2u^2} \right) \ln(1 + 4u^2) \right] \\ &\times \left[12u^2 - 2 - \frac{16u^4}{3} - 16u \arctan 2u + \left(6 + \frac{1}{2u^2} \right) \ln(1 + 4u^2) \right], \end{aligned} \quad (25)$$

$$\begin{aligned} \bar{E}_n(\rho_n) &= \frac{g_A^6 m_\pi^9 u}{18(4\pi f_\pi)^6 \Delta^2} \left[\frac{4u^4}{3} - 6u^2 + 2 + 10u \arctan 2u - \left(\frac{9}{2} + \frac{1}{2u^2} \right) \ln(1 + 4u^2) \right] \\ &\times \left[12u^2 - 2 - \frac{16u^4}{3} - 16u \arctan 2u + \left(6 + \frac{1}{2u^2} \right) \ln(1 + 4u^2) \right]. \end{aligned} \quad (26)$$

The last 1-ring diagram in Fig. 10 can be treated in the same way as the zig-zag diagram in Fig. 8. One finds the following double-integral representation for its contribution to the energy per particle of nuclear and neutron matter:

$$\begin{aligned} \bar{E}(\rho) &= \frac{3g_A^6 m_\pi^9}{(4\pi f_\pi)^6 \Delta^2 u^3} \int_0^u dx \int_0^u dy \left\{ \frac{5}{4} G_S(x) G_S(y) [4xy - L] + \frac{5}{8} G_S(x) G_T(y) \right. \\ &\times \left[\frac{3x}{y} (1 + x^2) - 5xy + \frac{L}{4} \left(2 + 6x^2 - 3y^2 - \frac{3}{y^2} (1 + x^2)^2 \right) \right] \\ &\left. + \frac{3}{8} G_T(x) G_T(y) \left[xy - \frac{3x}{y} (1 + x^2) + \frac{L}{4} \left(\frac{3}{y^2} (1 + x^2)^2 + 2 - 3x^2 \right) \right] \right\}, \end{aligned} \quad (27)$$

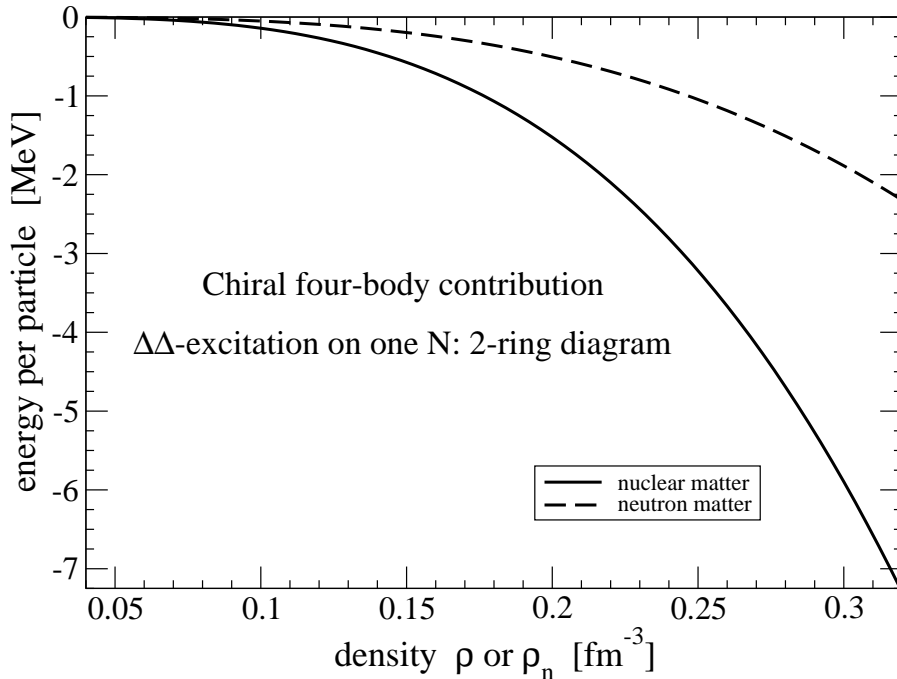


Figure 11: Δ -induced chiral four-body contributions to the energy per particle of nuclear and neutron matter: 2-ring diagram.

$$\begin{aligned}
\bar{E}_n(\rho_n) = & \frac{g_A^6 m_\pi^9}{24(4\pi f_\pi)^6 \Delta^2 u^3} \int_0^u dx \int_0^u dy \left\{ G_S(x)G_S(y) [4xy - L] + G_S(x)G_T(y) \right. \\
& \times \left[10xy - \frac{6x}{y}(1+x^2) + L \left(\frac{3}{2y^2}(1+x^2)^2 - 1 - 3x^2 + \frac{3y^2}{2} \right) \right] \\
& \left. + \frac{1}{5}G_T(x)G_T(y) \left[2xy - \frac{6x}{y}(1+x^2) + L \left(1 - \frac{3x^2}{2} + \frac{3}{2y^2}(1+x^2)^2 \right) \right] \right\}, \quad (28)
\end{aligned}$$

with the logarithmic function L defined in eq.(19). Note that the peculiar numerical coefficients entering the contact-vertex eq.(24), in particular the quark-model ratio $1/5$, have all disappeared in the final expressions for $\bar{E}(\rho)$ and $\bar{E}_n(\rho_n)$ in eqs.(25-28).

Numerical results for the energy per particle of nuclear and neutron matter as they arise from the double Δ -induced long-range four-nucleon interaction are shown in Figs.11,12. One observes attractive contributions from the 2-ring diagram which, in the next step, get nearly cancelled by repulsive contributions from the 1-ring diagram. After this balance the differences between nuclear and neutron matter which are individually visible in Figs.11,12 have essentially disappeared. The basic reason for the small net result in comparison to section 3 is the absence of a 3-ring diagram (with its large spin-isospin weight factor) and the lower number of subsequent diagrams. The pattern of alternating and largely compensating 3-ring, 2-ring and 1-ring contributions shown in Figs.5,7,9,11,12 is specific for the three-pion exchange four-nucleon interaction with two-fold Δ -excitation considered here. When using fully antisymmetrized many-nucleon forces [7, 9] this merely technical decomposition into different ring diagrams does not come into play at all.

5 Combined results and discussion

After having evaluated various classes of long-range four-nucleon correlations in nuclear and neutron matter in the previous sections let us now draw a balance. The summed result of

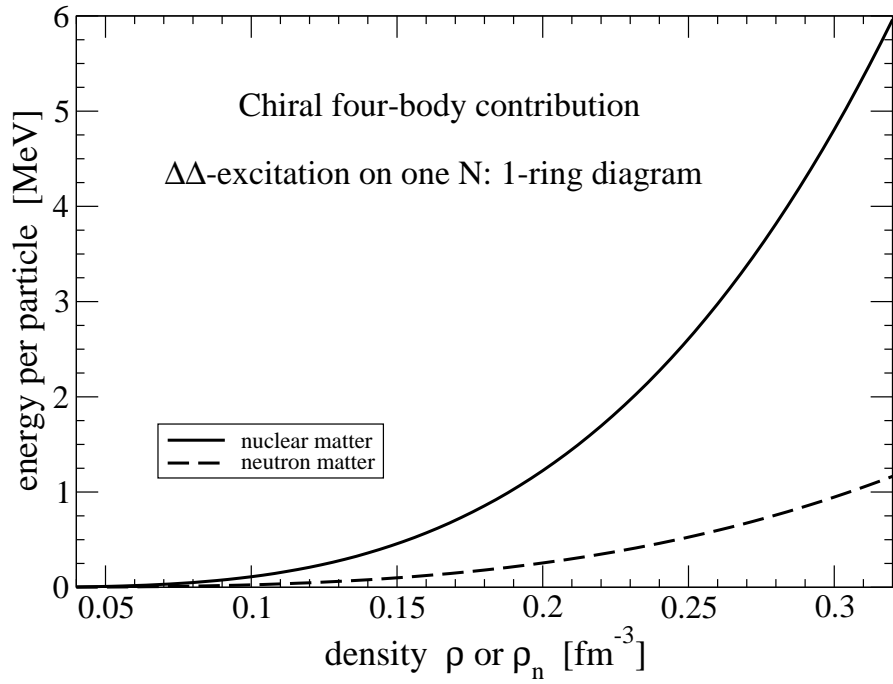


Figure 12: Δ -induced chiral four-body contributions to the energy per particle of nuclear and neutron matter: 1-ring diagram.

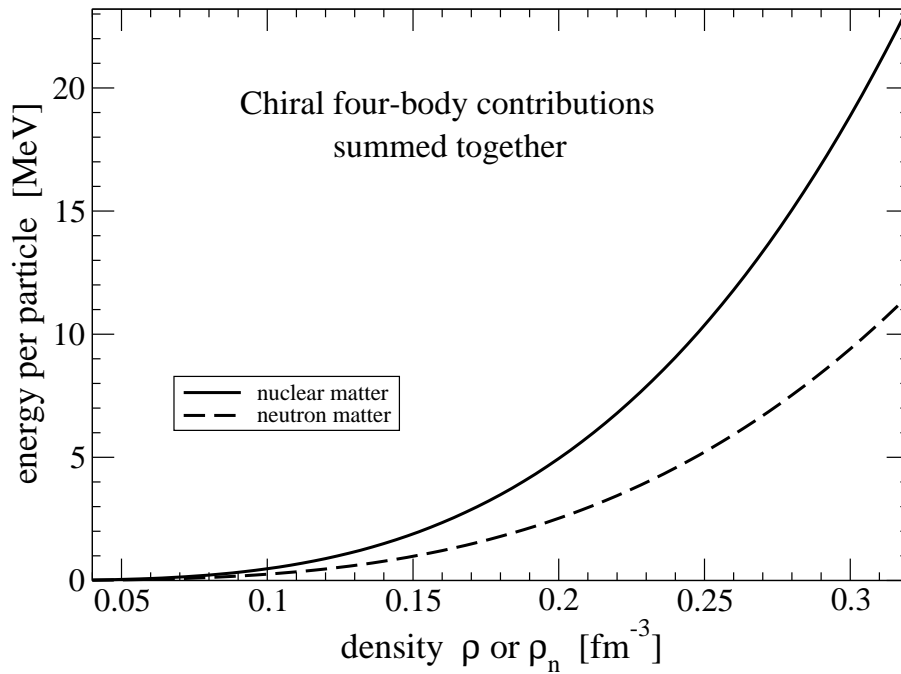


Figure 13: Chiral four-body contributions to the energy per particle of nuclear and neutron matter summed together.

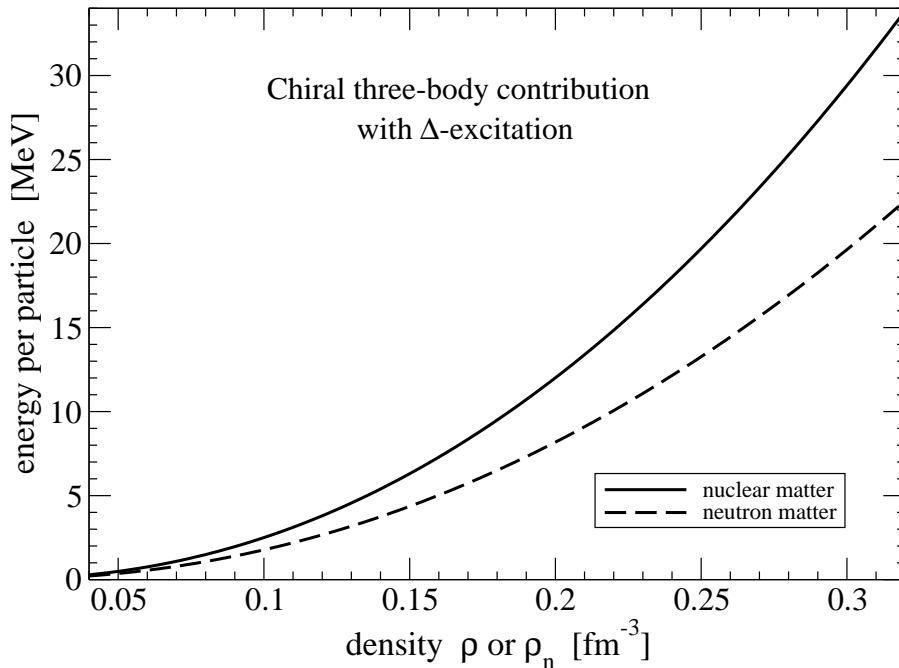


Figure 14: Three-body contributions to the energy per particle of nuclear and neutron matter arising from two-pion-exchange with Δ -isobar excitation.

all these contributions is shown in Fig. 13. For isospin-symmetric nuclear matter one finds at saturation density $\rho_0 = 0.16 \text{ fm}^{-3}$ a moderate repulsive contribution to the energy per particle of 2.35 MeV. However, the corresponding curve for $\bar{E}(\rho)$ rises strongly with the density and reaches the value 23.3 MeV at $2\rho_0 = 0.32 \text{ fm}^{-3}$. One should note that in this density range, $0 < \rho < 2\rho_0$, a realistic nuclear matter equation of state resides in the binding regime with a negative energy per particle. A mere addition of long-range four-nucleon correlations as given by the full line in Fig. 13 would produce enormous distortions. In pure neutron matter the long-range four-body correlations come out about half as large (see dashed line in Fig. 13). To put it into proportion, a value of $\bar{E}_n(2\rho_0) = 11.6 \text{ MeV}$ amounts to about 1/4 of what sophisticated neutron matter calculations [15] give at that density. It is also interesting to compare with the three-body correlations arising from 2π -exchange with (single) Δ -excitation in the same framework. The corresponding analytical formulas for $\bar{E}(\rho)$ and $\bar{E}_n(\rho_n)$ are written in eqs.(5,6,43,44) of ref.[16] and the associated numerical results are reproduced here in Fig. 14. By comparison with Fig. 13 one observes that for isospin-symmetric nuclear matter these long-range three-body correlations are at $2\rho_0$ about a factor 1.5 larger than the four-body correlations, whereas in pure neutron matter the relative factor between both is about 2. Note also that three-body and four-body correlations grow approximately quadratically and cubically with the density, respectively. The hierarchical order of multi-nucleon forces is therefore manifest for the long-range components considered in this work. Obviously, it gets more pronounced the lower the density (ρ or ρ_n) is.

In a recent work by the Darmstadt-Ohio group [9] a calculation of the neutron matter equation of state $\bar{E}_n(\rho_n)$ with inclusion of the subleading chiral three-nucleon forces has been performed for the first time. These authors find relatively large attractive contributions, which reach about -4 MeV at the highest considered density $\rho_n = 0.2 \text{ fm}^{-3}$ (see Fig. 2 in ref.[9]). This value is to be compared with 2.5 MeV repulsion due to chiral four-body correlations studied in the present work. It is therefore conceivable that substantial cancellations will occur among these novel higher order correlations. It remains as a future task to demonstrate the expected cancellations at a quantitative level for pure neutron matter and also for isospin-symmetric nuclear matter.

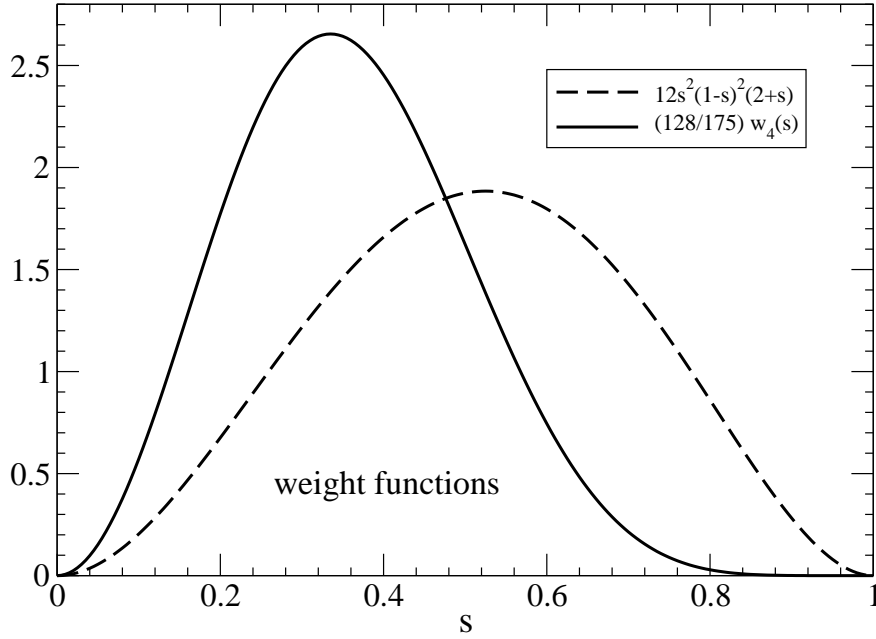


Figure 15: Weight functions for integrals over two and four Fermi spheres, respectively. The area under both curves is equal to 1.

Appendix: Reduction of integrals over Fermi spheres

In this appendix we collect several formulas which are useful for reducing integrals over (multiple) Fermi spheres. If the integrand depends only on the magnitude of the momentum transfer, the following reduction formula holds:

$$\int_{|\vec{p}_{1,2}| < k_f} \frac{d^3 p_1 d^3 p_2}{(2\pi)^6} F(|\vec{p}_1 - \vec{p}_2|) = \frac{k_f^6}{3\pi^4} \int_0^1 ds s^2 (1-s)^2 (2+s) F(2sk_f). \quad (29)$$

The weight function $s^2(1-s)^2(2+s)$ is slightly asymmetric about the midpoint $s = 1/2$ and it reaches its maximum at $s = (\sqrt{4.2} - 1)/2 = 0.5247$. These features are exhibited by the dashed line in Fig. 15. In order to give a geometrical interpretation of this weight function, we note that the overlap volume of two unit-spheres with their centers displaced by $2s$ is $2\pi(1-s)^2(2+s)/3$.

Pions with their momentum-dependent interactions lead often to the following tensorial integral over a Fermi sphere of radius k_f :

$$\int_{|\vec{p}_1| < k_f} \frac{d^3 p_1}{(2\pi)^3} \frac{(\vec{p} - \vec{p}_1)_i (\vec{p} - \vec{p}_1)_j}{m_\pi^2 + (\vec{p} - \vec{p}_1)^2} = \frac{m_\pi^3}{48\pi^2 x} \left\{ \delta_{ij} G_S(x, u) + (3\hat{p}_i \hat{p}_j - \delta_{ij}) G_T(x, u) \right\}. \quad (30)$$

By contracting this equation with δ_{ij} and $3\hat{p}_i \hat{p}_j - \delta_{ij}$ the functions $G_S(x, u)$ and $G_T(x, u)$ can be calculated separately as simple scalar integrals over a Fermi sphere $|\vec{p}_1| < k_f$. The dimensionless variables on the right hand side are $x = |\vec{p}|/m_\pi$ and $u = k_f/m_\pi$. The explicit analytical expressions for the functions $G_{S,T}(x, u)$ involving arctangents and logarithms are given in eqs.(10,11), suppressing in the notation the second argument u .

Let us add a further remarkable reduction formula for integrals over four Fermi spheres. We assume a dependence of the integrand on the magnitude of the total momentum $|\vec{p}_1 + \vec{p}_2 + \vec{p}_3 + \vec{p}_4|$ only and derive the following reduction formula:

$$\int_{|\vec{p}_j| < k_f} \frac{d^{12} p}{(2\pi)^{12}} F(|\vec{p}_1 + \vec{p}_2 + \vec{p}_3 + \vec{p}_4|) = \frac{8k_f^{12}}{175(3\pi^2)^4} \int_0^1 ds w_4(s) F(4sk_f), \quad (31)$$

with the (non-smooth) weight function:

$$w_4(s) = 4s(1-s)^6(16s^4 + 96s^3 + 156s^2 + 56s - 9) + \theta(1-2s)s(1-2s)^6(36 + 77s + 24s^2 - 12s^3 - 4s^4). \quad (32)$$

This peculiar result for $w_4(s)$ has been obtained with Fourier transformation techniques and eq.(31) has been checked numerically for many examples of $F(4sk_f)$. By employing the Fourier representation of the delta-function $\delta^3(\vec{p}_1 + \vec{p}_2 + \vec{p}_3 + \vec{p}_4 - 4k_f\vec{s})$ the weight function $w_4(s)$ results with a multiplicative factor $\pi/14175$ from the integral $s^2 \int_0^\infty dq q^2 j_0(4sq)[j_1(q)/q]^4$, where $j_{0,1}(q)$ denote spherical Bessel functions. The weight function $w_4(s)$ is normalized to $\int_0^1 ds w_4(s) = 175/128$ and a quick analysis shows that it reaches its maximum value of 3.63 at $s = 0.335$. The asymptotic behavior is: $w_4(s) = 85s^2$ for $s \rightarrow 0$, and $w_4(s) = 1260(1-s)^6$ for $s \rightarrow 1$. These features are exhibited by the full line in Fig. 15. The two weight functions put side by side in Fig. 15 demonstrate furthermore that multiple Fermi sphere integrals are dominated by total momenta of the order of the Fermi momentum k_f .

Acknowledgement

I thank S. Fiorilla, A. Schwenk, W. Weise and A. Wirzba for valuable discussions and for specific advice.

References

- [1] E. Epelbaum, *Prog. Part. Nucl. Phys.* **57**, 654 (2006); and refs. therein.
- [2] E. Epelbaum, H.-W. Hammer and Ulf-G. Meißner, *Rev. Mod. Phys.* **81**, 1773 (2009).
- [3] R. Machleidt and D.R. Entem, *Phys. Rep.* **503**, 1 (2011).
- [4] S.K. Bogner, R.J. Furnstahl and A. Schwenk, *Prog. Part. Nucl. Phys.* **65**, 94 (2010).
- [5] S.K. Bogner, R.J. Furnstahl, A. Nogga and A. Schwenk, *Nucl. Phys.* **A763**, 59 (2005).
- [6] A. Nogga, S.K. Bogner and A. Schwenk, *Phys. Rev.* **C70**, 061002 (2004).
- [7] K. Hebeler et al., *Phys. Rev.* **C83**, 031301 (2011).
- [8] V. Bernard, E. Epelbaum, H. Krebs and Ulf-G. Meißner, *Phys. Rev.* **C77**, 064004 (2008).
- [9] I. Tews, T. Krüger, K. Hebeler and A. Schwenk, nucl-th/1206.0025; and refs. therein.
- [10] E. Epelbaum, *Phys. Lett.* **B639**, 456 (2006).
- [11] E. Epelbaum, *Eur. Phys. J.* **A34**, 197 (2007).
- [12] D. Rozpedzik et al., *Acta Phys. Polon.* **B37**, 2889 (2006).
- [13] A. Deltuva, A.C. Fonseca and P.U. Sauer, *Phys. Lett.* **B660**, 471 (2008).
- [14] S. Fiorilla, N. Kaiser and W. Weise, *Nucl. Phys.* **A880**, 65 (2012).
- [15] A. Akmal, V.R. Pandharipande and D.G. Ravenhall, *Phys. Rev.* **C58**, 1804 (1998).
- [16] S. Fritsch, N. Kaiser and W. Weise, *Nucl. Phys.* **A750**, 259 (2005).